Study of continuous cake pre-baking in a rectangular channel using ohmic heating

Monique Khodeir, Olivier Rouaud, Anthony Ogé, Vanessa Jury, Patricia Le-Bail, Alain Le-Bail

Study of continuous cake pre-baking in a rectangular channel using ohmic heating

Monique KHODEIR[a,c], Olivier ROUAUD[a,c,*], Anthony OGE[a,c], Vanessa JURY[a,c], Patricia LE BAIL[b,c], Alain LE BAIL[a,c]

[a] *Oniris, Université de Nantes, CNRS, GEPEA, UMR 6144, F-44000 Nantes, France*
[b] *INRAE, UR 1268, Biopolymères Interactions Assemblages, Rue de la Géraudière, BP 71627, F-44316 Nantes Cedex 3, France*
[c] *SFR IBSM 4202, INRAE-BIA, CNRS-GEPEA, Nantes, France*

ABSTRACT

An original device dedicated to additive manufacturing was developed to pre-bake cake batter. Its originality lies in the fact that pre-baking is ensured by ohmic heating implemented in a rectangular channel equipped with two parallel electrodes. Experiments and numerical studies were carried out and benchmarked. The rheological properties of the cake batter (non-Newtonian power-law fluid) and the influence of voltage and temperature on electrical conductivity were accommodated in the numerical model. Due to the low velocities of the very viscous products near the solid-liquid interface, it was found that the heterogeneity of the temperature at the nozzle outlet under continuous ohmic heating could lead to nozzle clogging when high temperatures are reached. Hot spots were identified in different areas of the channel, such as corners where the electric field is high and velocity is close to zero. A parametric study was performed on the impact of the thermophysical properties of the batter, showing that specific heat has a much greater impact than thermal conductivity on the accuracy of the temperatures computed. Analysis of the process parameters showed that a stronger electric field leads to a higher temperature gradient in the nozzle section. The temperature gradient decreases with electrode distance (d_{elect}) and nozzle width *(l)*. This model could be used to optimize the ohmic heating nozzle configuration, with the objective of obtaining a continuous flow of pre-baked cake batter, while preventing clogging. Such a system could be used as 3D printing head.

Industrial relevance:
Conventional 3D printing of bakery products is based on the deposition of a batter, followed by a baking. This study proposes an innovative approach based on a printing nozzle equipped with ohmic heating, with the objective of achieving a uniform temperature distribution and of obtaining high mass flow rate. Despite a significant temperature gradient in the baked batter at the exit of the nozzle, the obtained results showed that adjusting the nozzle geometry allows a reduction of the gradient. Further investigations are thus needed to reduce the temperature gradient and to accommodate expansion of the batter in the case of formulation using baking powder. The transfer of such concept for industry application may be doable in a close future.

Keywords: Continuous Ohmic Heating, Baking, Cake Batter, Modeling, Electrical Conductivity, Rheology

Nomenclature

A	Electrode cell area for electrical conductivity measurement (m^2)
C_p	Heat capacity ($J \cdot kg^{-1} \cdot K^{-1}$)
d_{elect}	Electrode nozzle distance (mm)
D_h	$(4 \times S_2)/P$, Hydraulic diameter (m)
I	Current (A)

k	Thermal conductivity ($W \cdot m^{-1} \cdot K^{-1}$)
K	Constant of Eq. (14) ($°C^{-1}$)
L	Nozzle length (mm)
l	Nozzle width (mm)
L_h	Hydrodynamic entry Length (m)
L_{elect}	Electrode cell distance for electrical conductivity measurement (m)
m_d	Mass of batter sample (kg)
m_i	Mass of batter when weighing immersed in oil (kg)
P	Nozzle perimeter (m)
m	Consistency index (Pa. s^n)
$\dot{m}$	$S_2 \times V_2$, Volume flow rate (kg. s^{-1})
n	Flow index (-)
P_r	$(\mu\ C_p)/k$, Prandtl number
$\dot{Q}$	Ohmic heating source ($W \cdot m^{-3}$)
S	Section (m^2)
S_2	nozzle surface in the normal direction of the flow (m^2)
T_{ref}	Reference temperature (°C)
T_{m-N}	Nozzle mean temperature (°C)
T	Temperature (°C)
V_1	Piston velocity (mm. s^{-1})
V_2	Batter velocity inside the nozzle (mm. s^{-1})
V	Voltage (V)
Greek letters	
σ	Electrical conductivity (S. m^{-1})
σ_{ref}	Reference electrical conductivity at T_{ref} (S. m^{-1})
ρ_{app}	Batter apparent density (kg. m^{-3})
ρ_{oil}	Oil density (kg. m^{-3})
μ	Viscosity (Pa. s)
Δp	Differential pressure (Pa)
Subscripts	
app	Apparent
d	Batter sample
elect	electrodes
h	Hydraulic, hydrodynamic
i	Immersed in oil
m-N	Nozzle mean value
oil	oil
ref	reference
1	Point to refer to piston region

2	Point to refer to nozzle region

1. Introduction

3D printing (3DP), also known as additive manufacturing (AM), has undergone rapid growth in the last few years, due to its large scope of application (Ali et al., 2016; Liu et al., 2018). It was first introduced by researchers from Cornell University, using hot-melt extrusion to create personalized chocolate products in complex 3D structures, using a Fab@home printer (Sun et al., 2015). 3D printing applied to food is based on different technologies, as recently reviewed by Le-Bail et al. (2020), and the most important applications are fused deposition modeling (FDM) and soft-material extrusion (Severini & Derossi, 2016). A variety of materials has been used to demonstrate food printing. Most of the existing publications linked to the 3D printing of baked products are based on the deposition of a batter baked after deposition. The earliest application of 3D printing focused on the printing of a "cake mix", by extruding a batter mixture that consisted of starch, sugar, corn syrup, yeast, and a cake frosting (Lanaro et al., 2017; Yang et al., 2001). However, the biggest challenges are ingredient mixing, the associated rheology, structure accuracy and shape-stability, compatibility with traditional food processing technologies (e.g. baking and drying), and printing speed. Usual approaches to solidify the structure are based on cold extrusion, followed by a post-processing step. Lipton et al. (2010) demonstrated that traditional cookie recipes were compatible with 3D printing. However, extruded products do not retain their shape and structure after post-processing (e.g. baking), due to the presence of high amounts of fat. Two methods can be used to solve the shape stability problem: additives and recipe control (Lille et al., 2018; Lipton et al., 2015, 2010), but solutions consisting of pre-baking the product have not been explored. The challenge consists in solidifying the product while ensuring its flow. Using a conventional heating system (based on hot walls) would yield a batter to crumb transition starting at the wall with a progressive transfer towards the center of the flow. This may cause several problems, in particular because the baked batter (crumb) would be much harder than the unbaked batter at center of the flow.

This paper focuses on new process solutions like solidifying while printing to prevent shape destruction by implementing ohmic heating in the nozzle head. Ohmic heating (OH) is a thermal process consisting of the internal generation of heat by the passage of an electric alternating current (AC) through a medium with electrical resistance, such as food. In contrast to conventional heating (CH), where the heat of a hot surface is conducted from the outside of a food to its inside, OH is considered to induce heat within the entire mass, i.e. uniformly through the food (Leizerson & Shimoni, 2005). OH should allow for higher mass flow rate of the printing nozzle, accurate control of the temperature and improvement of the energy efficiency. This concept is not new and was used in the early 20th century for the electric pasteurization or sterilization of milk and other pumpable foods (viscous or liquid foods), such as fruit and vegetable products (juices, purees, pulps, etc.), and aseptic packaging (De Alwis & Fryer, 1990b; Sarkis et al., 2013; Yildiz & Guven, 2014). OH was also applied to solid foods and significant differences between OH and CH were highlighted. Textural changes can occur following the microscopic and macroscopic changes in food products (Gavahian et al., 2019). The kinetic of textural softening and the product texture could be affected by volumetric heating at high rate. Kamali & Farahnaky, (2015) have also shown that ohmically processed vegetables were characterized by a high textural cohesiveness. OH provides food industries with several benefits such as saving in process time and energy. One of the main advantages is the rapid and relatively uniform heating achieved (Marra et al., 2009). Contrary to classical heaters, whose heating is not homogeneous, due to the nature of heat migration, OH can achieve homogenous warming impossible to accomplish with classical heaters (Shynkaryk & Sastry, 2012). One important key for successful OH is first to identify possible hot and cold spots, in order to eliminate them and ensure the uniformity of heating or to achieve the desired temperature profile.

Several studies on ohmic cooking have been performed, but few of them have focused on bakery products. The first application in baking was carried out on bread by Baker, (1939), whose aim was to obtain a baked dough without temperature gradients. Gally et al., (2016) showed the interest of using OH to bake crustless bread in batch conditions. Studies on several applications of OH to the batch baking of cake have been published such as (e.g. Deleu et al., 2019; Luyts et al., 2013; Masure et al.,

2019). However, to our knowledge, the baking of bakery products by OH in continuous conditions has never been studied. In such conditions, with a strong change in the rheological properties of the batter during the batter-crumb transition, OH appears as much more adapted than CH using a heated channel.

Mathematical modeling is a valuable tool for the development, understanding, and validation of these emerging thermal technologies (Tijskens et al., 2001). It allows evaluation of the influence of key variables such as electrical field strength and sample conductivity. Initial models of ohmic processes, mainly two-dimensional systems, were developed for continuous flow systems, using liquid-solid mixtures (Marra et al., 2009). Numerical modeling is essential to understand the OH process, due to the difficulty of measuring real internal temperatures during continuous flow, because of the presence of a strong electric field (Sastry & Palaniappan, 1992). Mathematical models were developed and validated experimentally to study the heating patterns of solid–liquid mixtures in static ohmic heaters (De Alwis & Fryer, 1990a; Salengke & Sastry, 2007; Sastry & Palaniappan, 1992; Shim et al., 2010; Zhang & Fryer, 1993). On the other hand, numerical models for multiphase foods in continuous ohmic heaters have been developed, due to the complexity of the parameters (Chen et al., 2010; Choi et al., 2014; Sastry, 1992). Some works have concerned the continuous OH treatment of highly viscous fluids (Shynkaryk & Sastry, 2012). The numerical results have shown the importance of the OH chamber geometry, as it influences both current and fluid flow patterns and thus the uniformity of heating.

The present study focuses on a new approach, consisting of the partial baking of a cake batter, using ohmic heating embedded inside the printing nozzle head. This study is comprised of three main parts. First, an original printing nozzle device, based on a rectangular canal, was developed to obtain a cake batter pre-baked by OH. Second, the thermophysical and electrical properties of the cake batter were determined, and then a numerical model was developed to model OH in continuous flow, with the objective of understanding the links between the thermophysical properties, the channel geometry, and the temperature profile in the printing nozzle. After validating the numerical model, additional simulations were carried out to establish recommendations to ensure convenient cake pre-baking by continuous OH.

2. Materiel and Methods

2.1. Materials

2.1.1. Rectangular nozzle description

A rectangular nozzle was chosen because of its ease of development and versatility. 3D geometry was plotted on Autodesk® Inventor® 2015; the drawing of the nozzle is presented in Fig. 1. It consists of: 1) two parallel stainless steel electrodes (red), enclosed in 2) two rectangular polycarbonate plates (gray), separated by 3) two polycarbonate beams (green) 0.105 m long, with variable width and thickness to allow calibrating the nozzle dimension, and finally, 4) a channel support also made of polycarbonate (A) and (B). Fig. 1 (C) shows the nozzle dimensions, where the nozzle length, L, is equal to 105 mm. The total width of the device, b, is equal to 80 mm; the thicknesses of the electrodes and the polycarbonate plates are equal to 1 mm and 10 mm, respectively. The nozzle section depends on the width, l, and on the distance between the electrodes, d_{elect}, set at 4 cm and 1 cm, respectively, for this paper.

2.1.2. System description

The complete experimental set-up is presented in Fig. 2 (A). A drive motor (H T23-400D, ORIGA System plus, USA) was used to (1) impose the displacement of the piston at a constant velocity, (2) ensure a flow of batter in the cylindrical container (3), and then in the rectangular nozzle (4). The nozzle was equipped with electrodes to heat and pre-bake the cake batter.

The voltage applied between the electrodes (ohmic heating) by the voltmeter (a) (Fluke 45 dual display multimeter, USA) was controlled by an autotransformer (d) (DEREIX S.A, Paris, rotortransfo 120 NC, reference R.212). All the data collected from the experiments, especially the temperature variations measured between the inlet and the outlet, were logged by a data logger (c) (AOIP, France) and stored in the PC (f) (logidat program, Samsung computer). The current flowing through the cake batter was recorded with an ammeter (b) (Multimeter MN 5128, AOIP Mesures, France).

During each experiment, the velocity applied by the piston (2) and the voltage between the electrodes were constant, and the temperature of the batter through the nozzle increased due to ohmic heating.

2.1.3. Experimental procedure and outlet temperature

All the experiments were conducted in such a way that the batter passing through the nozzle did not solidify. The nozzle dimensions were mentioned in section 2.1.1, and the process parameters were set to 65 V for the voltage and V_1 = 0.1 mm/s for the piston speed. Four thermocouples (T_1 to T_4) were installed at the outlet of the nozzle (Fig. 2B), and one thermocouple T_5 at the inlet, to measure the variation of temperature along the nozzle. Four experiments were carried out with the same process parameters, and the temperature of the cake batter at the inlet was between 16 °C and 22 °C.

2.1.4. Cake batter sample preparation

Cake batter was prepared based on the recipe and cake-making method of Hesso (Hesso et al., 2014), except that no baking powder was used. The recipe used for the reference cake batter is given in Table 1. The ingredients of each formula were mixed in a KitchenAid (KSM90, KitchenAid, St. Joseph, MO, USA) in two stages to obtain the final cake batter. In the first stage, sugar, fat, and liquid egg were mixed for 2 min at average speed 6, then the wheat flour and salt were added and mixed in the second stage for 3 min at high speed 8.

Table 1
Cake batter recipe.

Ingredient	**Origin**	**Percentage wb(%)**	**Water content (% db) [ISO 712 : 2001(1998)]**
Wheat Flour T55	Petits moulins de France		
Sugar (S)	Saint Louis, France	25	
Fat (FA)		20	
Liquid Egg (E)	Ovoteam, France	25	
Salt (SA)	Cerebros, Esco France s.a.s, France		

2.2. Batter characterization

2.2.1. Ohmic heating system and measurement of electrical conductivity

A literature review showed the importance of controlling electrical conductivity during OH of a food product. In order to correctly design and control the batter cooking process, it was essential to determine the batter's electrical conductivity under different experimental conditions. All experiments were carried out in triplicate.

The ohmic cell, used to calculate the electrical conductivity of liquid products, was adapted from Gally et al. (2016), with small changes in cell material and dimensions. The short cell was replaced by a new polyacetal with an internal diameter of 29 mm and an external diameter of 42 mm.

The impact of electric voltage on the electrical conductivity of the cake batter was monitored with AC voltages (50 Hz) of 100 V, 150 V, and 200 V (22 V/cm, 33 V/cm, and 48 V/cm). The time–temperature data were plotted to obtain the ohmic heating curves for the batter. Electrical conductivity was plotted against the corresponding temperature to obtain the electrical conductivity curves. Electrical conductivity was measured using the following equation:

$$\sigma = {(L_{elect} \times I)}/{(A \times V)} \quad (1)$$

L_{elect}/A denotes the cell constant and is equal to 67.72 m^{-1}. It is calculated from a calibration, using the method of Olivera et al. (2013). Solutions of potassium chloride and sodium chloride were used as references, for which their electrical conductivities are known for their temperatures and concentrations.

2.2.2. Measurement of thermal conductivity and heat capacity

The thermal conductivity of the cake batter was measured based on the method proposed by Sweat & Parmelee (1978) and also used by Jury et al. (2007), using a line-heat source probe. The probe consists of a hypodermic needle with an external diameter of 0.7 mm and a length of 3.5 cm, containing a heating wire and a K-type thermocouple (OMEGA, Stamford, CT, USA). The thermal conductivity measurements were performed at different temperatures, by placing the samples in a climatic chamber (Froilabo, Meyzieu, FRANCE).

The heat capacity was measured by micro-calorimetry, with a micro DSC VII (SETARAM, Caluire, FRANCE), calibrated against the specific heat of saphir. Around 100 mg of batter was installed in a stainless steel pan, which was hermetically closed. A heating rate of 1 °C/min was used from *10* to *120 °C*; the integration of the thermogram provided an enthalpy function whose derivative yielded a specific heat function (provided as a function of temperature). All the thermal conductivity and heat capacity experiments were carried out in triplicate.

2.2.3. Density

A densimetric method was used to calculate the apparent density of the cake batter (Baker & Mize, 1946). A 500 ml beaker was filled with rapeseed oil (density: 935.5 kg/m^3) and placed on a scale. A holder was maintained in the oil, and the tare was set. The batter was weighed on the scale and then immersed in the oil. Its apparent density was calculated using the following equation:

$$\rho_{app} = m_d \times \rho_{oil}/m_i \quad (2)$$

The density of the oil was determined by the weight/volume method, using a 45.28×10^{-6} m^3 glass cylinder. The cup was filled with oil, leveled on the surface using a spatula, and weighed on an analytical balance. This technique yielded a true batter density, accommodating the possible presence of gas entrapped in the batter during mixing.

2.2.4. Rheological properties

The hydro-thermal transformations undergone by starch and gluten are the origin of the evolution of the rheological properties of a dough during cooking (Bloksma, 1980). Many models have been developed, leading to a large number of phenomenological models for dough viscosity (Zhou, 2004).

The apparent viscosity of batter was determined using a rotational viscometer, 'VT550 RHEOWIN' (HAAKE, France). The fluid was placed between two coaxial cylinders with a well-defined imposed shear rate, and the resulting shear stress was measured. Rheological measurements were performed between 25 and 95 °C, with a precision close to ±1% for the apparent viscosity, using a Ministat 230/Huber with a step of 10 °C. The variation of the consistency index, *m,* and the flow index, *n,* of the batter was determined for a shear rate between 0.9 and 150 s^{-1} in 2 min. These experiments were performed in triplicate.

2.3. Numerical models

2.3.1. 2D and 3D geometries

2D and 3D numerical models were developed on COMSOL Multiphysics 5.4, to study the temperature profile of the cake batter in continuous flow at the nozzle outlet.

The 3D model is represented with symmetry along the xz-plane, to decrease simulation time. The 2D geometry shows the nozzle in the xz-plane.

A mesh independency study for a laminar non-Newtonien fluid flow was performed to determine its effects on the CFD (Computational fluid dynamics) simulation results. It was clear that the simulation time was highly dependent on the number of mesh nodes, and a compromise had to be found between the grid-independent solution and the calculation time.

The numbers of domain elements chosen for the 2D and 3D models were equal to 3341 and 36238, for simulation times of 302 s and 1407 s, respectively.

2.3.2. Governing equations

Due to the existence of a strong electric field inside the nozzle, the temperature profile was very difficult to measure experimentally. The fluid temperature was measured at three points at the outlet of the nozzle. To carry out a stricter validation of numerical models, we made the choice to study the non-stationary flow, in order to obtain the evolution of the temperature at the nozzle outlet.

Navier–Stokes equations were used to describe the incompressible fluid flow, in which flow behavior is governed by:

$$\rho\ \partial u/\partial t + \ \rho\ (u.\nabla)u = \nabla.[-pI + \mu(\nabla u + (\nabla u)^T)]\ +\ F \quad (3)$$

where u is the velocity field. From left to right, the different terms in the equation above correspond to the inertial forces, the pressure forces, the viscous forces, and the gravitational force applied to the fluid ($F = -\rho g$).

Besides the Navier-Stokes equation, the continuity equation was also solved:

$$\partial\rho/\partial t + \rho\nabla.(u) = 0 \quad (4)$$

where $\partial\rho/\partial t = 0$, because it is considered to be an incompressible fluid.

In the case of the continuous flow ohmic heating process, the product is subjected to temperature and shear-rate gradients. A power-law model is used to fit the batter viscosity:

$$\mu = m\,\dot{\gamma}^{(n-1)} \quad (5)$$

where μ is the viscosity, $\dot{\gamma}$ the shear rate, m the consistency index which is temperature dependent, and n the flow behavior index.

Heat transfer within the liquid sample was solved and based on the general heat equation with a source term:

$$\rho C_p\,\partial T/\partial t + \ \rho C_p u.\nabla T\ =\ \nabla.(k\nabla T) + \dot{Q} \quad (6)$$

where ρ is the density which is constant, C_p is the heat capacity at constant pressure, and k is the thermal conductivity. C_p and k are temperature dependent, and is the Ohmic heating power source. The heat, in Eq. (7) is generated by Joule effect, due to the dissipation of electrical energy into heat:

$$\dot{Q} = \ \sigma.|\nabla V|^2 \quad (7)$$

where $|\nabla V|$ represents the modulus of the gradient of electrical potential, and σ is the temperature-dependent electrical conductivity of the batter.

The electrical potential distribution within the batter was computed using the following Laplace equation:

$$\nabla.\sigma\nabla V = 0 \quad (8)$$

2.3.3. Boundary and initial conditions

A vertical natural convection condition was considered to exist at all the faces of the nozzle. The heat losses, due to convection phenomena between the nozzle and the ambience around the sample, take into consideration the external heat-transfer coefficient (h_{ext}), using COMSOL equations with q being the convection heat flux (W. m^{-2}):

$$q = h_{ext}\,(T_{ambient} - T) \tag{9}$$

The initial batter temperature is equal to T_i at $t = 0$ (0 - time injection), and the initial nozzle temperature is equal to $T_{ambient} = 20$ °C.

For the inlet flow conditions, it was shown that a uniform velocity profile at the inlet affects the temperature profile as well as the pressure drop along the nozzle. An analysis was performed to choose the right velocity profile at the nozzle inlet and to calculate the hydrodynamic entry length (L_h), Reynolds number (N_{GRe}), and pressure drop (Δp). The calculation was performed by considering the mean values of the different parameters at the mean nozzle temperature between the inlet and the outlet. The power-law Reynolds number used is:

$$N_{GRe} = 2^{(3-n)}\,\frac{\rho_{app}\,V_2^{2-n}\,{D_h}^n}{m\left(\frac{3n+1}{n}\right)^n} \tag{10}$$

The hydrodynamic entry length of this region was calculated from:

$$L_h = 0{,}05\,R_e\,D_h \tag{11}$$

The differential pressure of power-law non-Newtonian laminar flow is given by:

$$\Delta p = \frac{2^{n+2}\left(\frac{3n+1}{n}\right)^n L\,m\,V_2^n}{(D_h)^{n+1}} \tag{12}$$

Table 2 shows the analytical results used as boundary conditions for the numerical study.

Table 2
Rectangular nozzle – 65 V – V_1 = 0.1mm/s - analytical study.

Experience		$\mathbf{T_{m\text{-}N}}$ ***(°C)**	$\mathbf{N_{GRe}}$	$\mathbf{L_h}$ **(m)**	**Δp (Pa)**
$\mathbf{V_2}$ **(mm/s)**	**V**	**Expe**	**Eq (10)**	**Eq (11)**	**Eq (12)**
4	65	33.33	0.0023	1.8410^{-6}	1415.1

* mean nozzle temperature between the nozzle inlet and outlet.

The L_h ($1.84\ 10^{-6}$ m) obtained is much shorter than the nozzle length (0.105 m). As a consequence, the velocity was fully developed at the nozzle entrance section, as this region was much longer in the laminar flow condition than in turbulent flow (Cengel, 2008). The batter was characterized by a high Prandtl number (P_r = 421973), so that the flow is considered as thermally developing but hydrodynamically developed.

The wall conditions (solid – liquid interface). For the solid-liquid interface, no slip condition was considered to exist inside the nozzle, and the flow velocity in the immediate vicinity of the surface was assumed to be zero.

$$u = 0\ at\ \forall t \geq 0 \tag{13}$$

At the nozzle outlet section, the atmospheric pressure condition was set at $p = 0$ for any time above the initial time ($\forall t \geq 0$).

3. Results and Discussion

3.1. Effect of temperature and voltage gradient on electrical conductivity

Eq. (1) was used to determine the electrical conductivity of the cake batter and its evolution with temperature, as shown in Fig. 3 (A), at a voltage gradient of 50 V/cm.

Three stages are distinguishable. Zone 1 shows a polynomial curve of the second degree ($R^2 >$ 0.999), before starch gelatinization, from 26°C to 80°C; at this stage, the variation of electrical conductivity can be calculated, using a reference temperature, and expressed by Eq. (14). These results can be compared with those of Gally et al. (2016), who observed a linear variation of electrical conductivity, before starch gelatinization, for bread dough. Zone 2 begins at just below 80 °C, which represents the temperature at the beginning of starch gelatinization. From there, the rate of increase of electrical conductivity decreases strongly, until the temperature reaches 98°C, and at some stage, it becomes almost constant. Zone 3 shows a linear variation of electrical conductivity, with a slope different from that of zone 1. Similarly, Gally et al. (2016) obtained a linear pattern after gelatinization, with a different slope ($d\sigma/dT$), and attributed it to a change in the product.

The changes in the electrical conductivity of batter with temperature, during ohmic heating at three different voltage gradients, are shown in Fig. 3 (B). For a voltage gradient of 48 V/cm, the onset temperature of starch gelatinization was 80 °C, that of 33 V/cm was 90°C, and that of 22 V/cm was 100°C. These experiments showed that electrical conductivity increases with voltage gradient. Similar observations were reported for tomato juice in the range of 50–70 V/cm (Srivastav & Roy, 2014), and for apricot and peach juices in the range of 20–70 V/cm (Icier & Ilicali, 2005). As the voltage gradient increased, the heating time of the cake batter, required to reach the prescribed temperature, decreased. It was found that the ohmic heating time increased by up to 3.6 times, when the voltage gradient was decreased from 48 to 22 V/cm (Fig. 3C).

Electrical conductivity was modeled in zone 1 (before starch gelatinization) and can be written as follows:

$$\sigma = \sigma_{ref}\left(1 + K'\left(T - T_{ref}\right)^2 + K(T - T_{ref})\right) \quad (14)$$

where K and K' are constants, and T_{ref} and σ_{ref} are the reference temperature and electrical conductivity, respectively. Their values, at the three different electric voltages, are presented in Table 3. Fig. 3 (B) was used to model the variation of electrical conductivity with temperature at different voltages.

Table 3
Values of reference temperature, electrical conductivity, and constants K and K'.

Parameter	200V	150V	100V
$\mathbf{T_{ref}}$ (°C)	26.3	26.3	26.3
$\boldsymbol{\sigma_{ref}}$ (S/m)	0.048	0.051	0.055
K ($°C^{-1}$)	0.04	0.034	0.024
K' ($°C^{-2}$)	3.5410^{-4}	2.110^{-4}	1.4710^{-4}

3.2. Thermophysical properties of cake batter

3.2.1. Viscosity profile

Fig. 4 (A) and Fig. 4 (B) show the data, in logarithmic form, for the cake batter sample at a reference temperature of 25°C, and at different temperatures (35°C, 45°C, 75°C, and 85°C), respectively, where the shear rate varied from 0.9 to 150 s^{-1}. It was found that the power law fits the apparent viscosity behavior very well (r^2=0.99). The results illustrate the power-law non-Newtonian behavior of the cake batter. It is clear, in Fig. 4 (B), that the viscosity decreases, as expected (Bloksma, 1980), when the batter temperature increases at constant shear rate, before the gelatinization onset temperature. At a shear rate of 0.5 s^{-1}, the viscosities are equal to 1.4 and 0.8 Pa.s, at 25 °C and 75 °C, respectively. After gelatinization at 85°C, for the same shear rate of 0.5 s^{-1}, the viscosity increases again and is equal to 0.95 Pa.s.

Flow index, *n,* is equal to 0.6 ± 0.05 and is considered constant. The consistency index, *m,* is variable with temperature; it is equal to the viscosity, for a shear rate of 1 s^{-1}, as shown in Fig. 4 (C). Its evolution as a function of temperature is represented by Eq. (15).

$$m = 9 \times 10^{-5} \times T^3 - 0{,}0063 \times T^2 - 0{,}6672 \times T + 58{,}203 \quad (15)$$

It can be seen, in Fig. 4D, that the viscosity decreases with temperature at a fixed shear rate, until it reaches the gelatinization temperature. After that, it increases with temperature up to 95°C at a different shear rate. The viscosity decreases when the shear rate increases at constant temperature. At 25°C, it is equal to 18 and 12 Pa. s, at shear rates of 10 and 30 s^{-1}, respectively.

3.2.2. Density, heat capacity, and thermal conductivity

The cake batter density *(ρ)* was found to be 970 ± 8 kg. m^{-3}. The cake batter thermal conductivity vs. temperature could be modeled using Eq. (16); the limit of validity of this equation is 85°C, which is the gelatinization onset temperature.

$$k(T) = 3{,}8 \times 10^{-5} \times T^2 - 1{,}27 \times 10^{-3} \times T + 0{,}21 \quad (16)$$

The evolution and uncertainty of the cake batter's thermal conductivity and heat capacity with temperature are presented in Fig. 5.

Heat capacity and thermal conductivity are responsible for the considerable non-linearity of the numerical model, due to their temperature dependence.

3.3. Comparison between numerical simulation and experimental results

3.3.1 Outlet nozzle temperatures – voltage 65 V – velocity 4 mm/s

The experimental and simulation results for the outlet nozzle temperature vs. time are presented in Fig. 6. 2D and 3D simulations showed good agreement with the experiments for temperature T_1. In 2D geometry, edge temperature T_2 could not be determined, so a 3D simulation was necessary, which also showed a good correlation with the experiments.

The total injection time was 12 min at 65 V, with a batter velocity of 4 mm/s. When the steady state was reached after almost 7 min of injection, the results showed a temperature difference between T_1 and T_2 equal to 11°C. The transition phase, from 0 to 7 min, showed a small difference between the simulation and the experimental results and was composed of two parts. The first was from 0 to 1 min, where the linear temperature evolutions of T_1 and T_2 with time occurred at the same rate of 0.2°C/s. The second was from 1 min to 7 min, where the temperature evolution was polynomial, and the rate of increase of T_2 was faster than that of T_1. The temperature difference between T_1 and T_4, along the x axis, was almost insignificant and equal to 0.2°C.

In previous studies, Marra et al., (2009) and Gally et al., (2016) showed the advantage of using ohmic heating in static conditions, with a homogeneous temperature distribution with higher temperature at the center, due to volumetric heating from inside to outside. In the present study involving continuous OH, the temperature gradient between the center and the side of the rectangular channel was reversed, with hot spots in the corners of the channel. To better understand the reason for this heterogeneity, it is necessary to understand what occurs inside the nozzle, with the help of the numerical model.

Several simulation results are presented in Fig. 7. Fig. 7 (A) shows the volume electric field. The points where the electric field is the strongest are those at the edges of electrodes. At the center of the electrodes, the electric field is equal to 65 V/cm (in blue). At the bottom of the electrode (horizontal line, parallel to the y axis in Fig. 7 (A) and Fig. 7 (B)), the electric field varies between 200 and 250 V/cm, and at the edge line (or vertical line, light blue in Fig. 7 (A)) parallel to the z axis, it is equal to 100 V/cm.

The xy plane of the nozzle (Fig. 7B) also shows a strong electric field at the corner of the electrode (red zone). It can be seen that, inside the nozzle, the electric field passes through the batter in the perpendicular direction of the two electrodes. It can be seen that the electric field that crosses through

the nozzle body (polycarbonate) is negligible. The shear rate inside the nozzle depends on the velocity. Fig. 7 (C) shows that the lowest shear rate, which is almost equal to zero, is at the center of the nozzle, while the highest shear rate, which is parallel to the y axis and equal to 4.89 s^{-1}, is at the outlet edge of the nozzle.

The velocity profile tends to zero near the walls (solid-liquid interface) along the y and x axes, as shown in Fig. 7 (D). The residence time and the difficulty to remove heat by convection close to the walls cause temperature heterogeneity and higher temperature at the wall interface. As expected, the latter along the y-axis could cause fouling by clogging, due to starch gelatinization in the batter, in the case of higher voltages.

It is important to note the temperature distribution in the xy plane, as shown in Fig. 7 (E). It is obvious that the highest temperatures are at the corners between the electrodes and the polycarbonate beam. The temperature near the electrodes in the x direction is lower than those near the wall in the y direction, although the velocity is zero for both. This could be explained as being due to the strong electric field at these corners (Fig. 7B), along with very high viscosity and zero velocity. Hashemi & Roohi, (2019), have performed numerical modeling of process and bacterial inactivation kinetics with ohmic heating. They have found that the initiation of temperature rise near the regions with high gradient values of electric field was predictable with CFD. Jun & Sastry, (2005) have also found that the electric field strength near the edges of electrodes goes close to the maxima: up to 4985 V/m in their 2D numerical study on the ohmic heating of foods inside a flexible package. They conclude that the electrode configuration could be optimized to ensure uniformity of heating.

In summary, the heterogeneity of temperature is a consequence due not only to zero velocity at the wall interfaces, but also to the hot spots that occur at the electrode corners, because of the strong electric field and the very low velocity at these points.

In this section, the model developed was validated successfully, showing good agreement between the experimental and predicted temperatures. The main goal here was to predict the temperature profiles of the cake batter inside the nozzle. The results showed heterogeneous temperatures that could cause nozzle clogging at higher temperatures. The challenge now was to flatten and even reverse the temperature profile, by trying different process parameters and by studying the effect of batter properties on the outlet temperature profile. To do that, it seemed necessary to study the influence of certain parameters, and to determine their relative impact on the computed values.

3.3.2. Parametric study

A parametric study was carried out to monitor the impact of the batter properties and nozzle dimensions on the computed temperatures. In this section, all the results were obtained for stationary flows.

A) Thermal conductivity

The effect of thermal conductivity was studied first. The results are shown in Fig. 8 (A). The experimental results showed that the thermal conductivity varied from 0.2 to 0.4 W/(m. K), for a temperature range of 24°C to 74°C. A reference value was set to 0.4 W/(m. K). When this value decreased by 50%, T_2 increased by 3%, and T_1 decreased by about 2.5%. When the thermal conductivity increased by 50%, T_2 decreased by 2%, and T_1 increased by 2%. It can be seen here that, at a higher thermal conductivity, T_1 at the center and T_2 at the near edge were reversed. It was observed that, when the thermal conductivity was increased by about 50%, the temperature gradient decreased by almost 5%. In summary, when the thermal conductivity increased, the temperature gradient between the center and the near edge decreased; this result was expected, since high thermal conductivity facilitates heat diffusion within the batter, resulting in better temperature equilibration during heat-up. In turn, a reduced temperature gradient was observed.

These results showed that the accuracy in determining the thermal conductivity of the batter had a minimal impact on the computed temperature, as a 50% increase in this property yielded only a 2% to 3% uncertainty in the temperatures.

B) Specific heat

The impact of specific heat was investigated in a similar way. It was observed that, when the specific heat increased, temperatures T_1 and T_2 tended to decrease, the lowest specific heat resulting, as might be expected, in the highest temperatures. When the heat capacity was decreased by 8%,

temperatures T_1 and T_2 increased by 4%, and when the heat capacity was increased by 19 %, T_1 and T_2 decreased by 7%. A further result was that the specific heat had no effect on the temperature gradient, because T_1 and T_2 were affected at the same rate.

The temperature profile was not reversed, as had been shown in the previous study on the impact of thermal conductivity. The main finding was that greater accuracy in the determination of specific heat was needed, compared to that for thermal conductivity. For example, a deviation of 8% for specific heat led to a 4% deviation in the computed temperatures. However, the accuracy of specific heat was sufficient to conveniently predict the profile temperatures.

C) Density

The reference density of the cake batter was 980 kg/m^3. The density of the gas-free batter (obtained by computation) was 1200 kg/m^3, thus indicating that the batter porosity was *24.3%.* For a gas-free batter, the temperature observed at the center (T_1) decreased from 37.7 °C to 34.6 °C, corresponding to a temperature difference of 8%. In contrast, when the batter density was decreased by 50% (from 980 kg/m^3 to 500 kg/m^3), it was observed that T_1 increased by about 13%, based on the initial batter temperature. Here also, T_1 and T_2 were found to change at the same rate with density. Unlike thermal conductivity, but like thermal capacity, the batter density did not flatten the temperature profile. However, it seemed to be important to determine the batter density with sufficient accuracy, at least greater than that of the thermal conductivity, but less than that of the specific heat.

D) Electrical conductivity and viscosity

Fig. 8 (B) shows a parametric study on electrical conductivity and its effect on the temperature profile. The extreme limits of its value were used. Three values were chosen (0.05, 0.125, and 0.2 S/m), It can be seen that the higher the electrical conductivity, the higher was the temperature gradient between T_1 and T_2. Electrical conductivity plays a major role in the efficiency of the heating process, especially for sweet products, which have a lower electrical conductivity than salty products. Further investigations should be carried out to assess the influence of the cake batter formulation on this property. The same study was performed on viscosity: three values were studied (40, 25, and 13 Pa. s), namely the limits of variation of the batter viscosity between 20°C and 95°C. The results showed no significant impact of viscosity on the temperature profile.

In summary on the impact of batter properties, this study showed the importance of precision in the determinations of electrical conductivity, specific heat, density, and thermal conductvity, as they have a strong impact on the batter temperature profile. Among all the thermophysical properties of the cake batter, thermal conductivity appeared to be the one that most influenced the temperature gradient (the difference between T_1 and T_2). By increasing this property, the temperature gradient decreased, but this change was not sufficient to reverse the temperature profile (the temperature distribution inside the nozzle). Furthermore, it was difficult to control these properties, because they are temperature dependent, making the solution impossible.

To summarize this section, it seemed to be difficult to change the temperature profiles by adjusting the thermophysical properties of the cake batter. Hence, this situation led to the idea of studying the process parameters.

E) Nozzle dimensions

Further work, based on parametric studies, was carried out to assess the effect of nozzle geometry on the temperature profile. To do this, different aspect ratios ($\alpha = d_{elect}/l$) and nozzle dimensions were studied. The temperature distribution at the nozzle exit was determined for several electric field strengths, for the same flow velocity $V_2 = 4$ mm/s. Three channel cross sections were used (presented in Table 4) to determine the effect of nozzle dimensions on the heterogeneity of the temperature along the nozzle outlet along the y-axis.

Table 4
Dimensions of nozzle sections.

	l (cm)	d_{elect} (cm)	α
Section 1	2	0.5	0.25
Section 2	4	1	0.25

Section 3	2	1	0.5

Fig. 9 shows the evolution of the nozzle outlet temperature, at 65 V/cm (A) and 100 V/cm (B), for three different nozzle sections, as a function of the dimensionless number $y^* = y/(l/2)$. When the voltage was increased from 65 V/cm to 100 V/cm, for the same nozzle section, T_1 and T_2 increased by 22% and 23.5%, respectively. It can be observed that the increasing rate of temperature T_2 was higher than that of T_1, which means that, at a stronger electric field, a higher temperature gradient was produced for the same section.

Fig. 9 (A) shows the effect of the nozzle section, at 65 V/cm, on the outlet nozzle temperature. Section 1 (green line), section 2 (red line), and section 3 (blue line) are presented, where section 1 and 2 had the same aspect ratio but different nozzle dimensions. At 65 V/cm, the temperature difference between T_1 (center) and T_2 (wall), for an aspect ratio of 0.5 (section 3), 0.25 (section 1), and 0.25 (section 2), were equal to 13 °C, 8.5 °C, and 15 °C, respectively. For 100 V/cm, the temperature differences between T_1 (center) and T_2 (wall) were equal to 18 °C, 12.5 °C, and 20 °C, respectively (Fig. 9B).

In summary, for different voltages, it was found that the aspect ratio affected temperature heterogeneity along the y-axis. For the same nozzle width l (section 1 and section 3), if the distance between the electrodes (d_{elect}) was decreased from 1 to 0.5, then the temperature difference also decreased from 13 °C to 8.5 °C, at 65 V/cm. In addition, for the same distance between the electrodes (section 2 and 3), when the nozzle width l was increased from 2 to 4, the temperatures difference increased from 13°C to 15°C, for 65 V/cm. Finally, for all the voltages, it was found that section 1 was the most efficient, as it yielded the minimal temperature difference for different voltages, but did not provide a flattened or reversed temperature profile (warmer temperature at the center than in the corners of the channel), which was our final goal, in order to print and pre-bake at the same time.

According to the parametric study, we observed that it was difficult to obtain a homogeneous temperature along the y-axis, by adjusting the dimensions of the nozzle section. Further investigations should be carried out with different configurations because some modifications could result in a reduction of the overheating as in (Shynkaryk & Sastry, 2012). Cooling of the containment walls of the nozzle, which is the practice for some larger industrial ohmic heating systems, could also be part of the solution (Quarini, 1995). As OH is based on volumetric heating from the inside to the outside, a simulation was performed, involving the cooling of the nozzle walls along the y-axis. The simulation in stationary mode, for 4 mm/s and 65 V, showed that we had to remove almost 840 W/m^2, which was equal to 4% of the total heat power produced in the product, on each side of the walls of the nozzle, in order to make the temperature almost homogeneous along the y-axis.

4. Conclusion

A new, innovative system was developed to study the possibility of pre-baking a cake batter in continuous flow, by implementing OH in a rectangular channel (nozzle). The study consisted of three main parts, namely the characterization of the thermophysical and electrical properties of the batter, experimental investigations, and CFD modeling of the experimental system, to better understand the links between the geometry of the printing nozzle, the physical properties of the batter, and the temperature distribution in the flow at the exit of the nozzle.

The experimental results showed considerable temperature heterogeneity along the y axis, which led to clogging at high temperatures. In-flow ohmic heating and batter baking resulted in heterogeneity in the temperature profile, and the temperature gradient in continuous ohmic heating was reversed, compared to the results obtained in batch conditions. Good correlation between results from simulations and experiments was observed, showing that the temperature heterogeneity along the y-axis was greater than that along the x-axis (electrodes distance). This finding was explained as being due to the presence of hot spots at the nozzle corners and electrode edges, where the electric field was higher than in the rest of the section of the nozzle. Also, the fact that the electrodes represented cold spots could explain why hot spots were found close to the corners of the nozzle, in the vicinity of the lateral walls, which were better insulated against heat transfer than were the electrode surfaces.

Different nozzle sections with aspects ratio of 0.25 and 0.5 (electrodes distances/width of nozzle) and voltage conditions were considered with the objective of mitigating the temperature gradient at the exit of the nozzle. The aspect ratio was found to affect temperature heterogeneity along the y-axis (channel width); decreasing the electrodes distance reduced the temperature gradient, while increasing the channel width yielded an increase of the temperature difference between the cold and the hot spots. Further investigations should be carried out with different nozzle-ohmic heating configurations, in order to find a suitable geometry capable of providing cake batter injection and pre-baking, without nozzle clogging. Short additional baking will be necessary to finish setting the structure after deposition. The effect of ohmic heating on food texture could be studied in the future once the partial baking process in a channel has been fully achieved. Once this will be achieved, application to 3D printing will be doable.

Acknowledgements

The authors would like to thank the Region Pays de la Loire (Food for tomorrow RFI) and ONIRIS-GEPEA for their financial support.

References

Ali, M. H., Mir-Nasiri, N., & Ko, W. L. (2016). Multi-nozzle extrusion system for 3D printer and its control mechanism. *International Journal of Advanced Manufacturing Technology*, *86*, 999–1010. https://doi.org/10.1007/s00170-015-8205-9

Baker J.C., M. M. D. (1946). Gas occlusion during dough mixing. *Cereal Chemistry*, *23*, 39–51.

Baker, J. C., & Mize, M. D. (1946). Gas occlusion during dough mixing. Cereal Chemistry, 23, 39–51.

Bloksma, A. H. (1980). Effect of heating rate on viscosity of wheat flour doughs. *Journal of Texture Studies*, *10(3)*, 261–269.

Cengel, Y. A. (2008). Internal forced convection. In *Cengel, Yunus A. (2nd Eds.), Solutions Manual for Introduction to Thermodynamics and Heat Transfer* (pp. 1–60). New York: The McGraw-Hill Companies, Inc.

Chen, C., Abdelrahim, K., & Beckerich, I. (2010). Sensitivity analysis of continuous ohmic heating process for multiphase foods. *Journal of Food Engineering*, *98*(2), 257–265. https://doi.org/10.1016/j.jfoodeng.2010.01.005

Choi, W., Lee, S. H., Kim, C.-T., & Jun, S. (2014). A finite element method based flow and heat transfer model of continuous flow microwave and ohmic combination heating for particulate foods. *Journal of Food Engineering*, *149*, 159–170. https://doi.org/10.1016/j.jfoodeng.2014.10.016

De Alwis, A. A. P., & Fryer, P. J. (1990a). The use of direct resistance heating in the food industry. *Journal of Food Engineering*, *11*(1), 3–27. https://doi.org/10.1016/0260-8774(90)90036-8

De Alwis, A. A. P., & Fryer, P. J. (1990b). A finite element analysis of heat generation and transfer during ohmic heating of food. *Chemical Engineering Science*, *45*(6), 1547–1559. https://doi.org/10.1016/0009-2509(90)80006-Z

Deleu, L. J., Luyts, A., Wilderjans, E., Van Haesendonck, I., Brijs, K., & Delcour, J. A. (2019). Ohmic versus conventional heating for studying molecular changes during pound cake baking. *Journal of Cereal Science*, *89*(January), 102708. https://doi.org/10.1016/j.jcs.2019.01.008

Gally, T., Rouaud, O., Jury, V., & Le-Bail, A. (2016). Bread baking using ohmic heating technology; a comprehensive study based on experiments and modelling. Journal of Food Engineering, 190, 176–184. https://doi.org/10.1016/j.jfoodeng.2016.06.029

Gavahian, M., Tiwari, B. K., Chu, Y. H., Ting, Y., & Farahnaky, A. (2019). Food texture as affected by ohmic heating: Mechanisms involved, recent findings, benefits, and limitations. In Trends in Food Science and Technology (Vol. 86, pp. 328–339). Elsevier Ltd. https://doi.org/10.1016/j.tifs.2019.02.022

Hashemi, S. M. B., & Roohi, R. (2019). Ohmic heating of blended citrus juice: Numerical modeling of process and bacterial inactivation kinetics. *Innovative Food Science and Emerging Technologies*, *52*(January), 313–324. https://doi.org/10.1016/j.ifset.2019.01.012

Hesso, N., Loisel, C., Chevallier, S., & Le-bail, A. (2014). Impact of Pregelatinized Starches on the

Texture and Staling of Conventional and Degassed Pound Cake. *Food Bioprocess Technol*, 7:2931. https://doi.org/10.1007/s11947-014-1308-8

Icier, F., & Ilicali, C. (2005). The effects of concentration on electrical conductivity of orange juice concentrates during ohmic heating. *European Food Research and Technology*, *220*(3–4), 406–414. https://doi.org/10.1007/s00217-004-1043-x

Jun, S., & Sastry, S. (2005). Modeling and optimization of ohmic heating of foods inside a flexible package. *Journal of Food Process Engineering*, *28*(4), 417–436. https://doi.org/10.1111/j.1745-4530.2005.00032.x

Jury, V., Monteau, J., Comiti, J., & Le-bail, A. (2007). Determination and prediction of thermal conductivity of frozen part baked bread during thawing and baking. Food Research International, 40(7), 874–882. https://doi.org/10.1016/j.foodres.2007.02.006

Kamali, E., & Farahnaky, A. (2015). Ohmic-Assisted Texture Softening of Cabbage, Turnip, Potato and Radish in Comparison with Microwave and Conventional Heating. Journal of Texture Studies, 46(1), 12–21. https://doi.org/10.1111/jtxs.12106

Lanaro, M., Forrestal, D. P., Scheurer, S., Slinger, D. J., Liao, S., Powell, S. K., & Woodruff, M. A. (2017). 3D printing complex chocolate objects: Platform design, optimization and evaluation. *Journal of Food Engineering*, *215*, 13–22. https://doi.org/10.1016/j.jfoodeng.2017.06.029

Le-Bail, A., Maniglia, B. C., & Le-Bail, P. (2020). Recent advances and future perspective in additive manufacturing of foods based on 3D printing. *Current Opinion in Food Science*, *35*, 54–64. https://doi.org/10.1016/j.cofs.2020.01.009

Leizerson, S., & Shimoni, E. (2005). Effect of ultrahigh-temperature continuous ohmic heating treatment on fresh orange juice. *Journal of Agricultural and Food Chemistry*, *53*(9), 3519–3524. https://doi.org/10.1021/jf0481204

Lille, M., Nurmela, A., Nordlund, E., Metsä-Kortelainen, S., & Sozer, N. (2018). Applicability of protein and fiber-rich food materials in extrusion-based 3D printing. *Journal of Food Engineering*, *220*, 20–27. https://doi.org/10.1016/j.jfoodeng.2017.04.034

Lipton, J., Arnold, D., Nigl, F., Lopez, N., Cohen, D., Norén, N., & Lipson, H. (2010). Multi-material food printing with complex internal structure suitable for conven- tional post-processing. In: 21st Annual International Solid Freeform Fabrication Symposium - an Additive Manufacturing Conference, SFF 2010, (pp. 809–8015). https://doi.org/10.1017/CBO9781107415324.004

Lipton, J. I., Cutler, M., Nigl, F., Cohen, D., & Lipson, H. (2015). Additive manufacturing for the food industry. *Trends in Food Science and Technology*, *43*(1), 114–123. https://doi.org/10.1016/j.tifs.2015.02.004

Liu, Z., Zhang, M., Bhandari, B., & Yang, C. (2018). Impact of rheological properties of mashed potatoes on 3D printing. *Journal of Food Engineering*, *220*, 76–82. https://doi.org/10.1016/j.jfoodeng.2017.04.017

Luyts, A., Wilderjans, E., Van Haesendonck, I., Brijs, K., Courtin, C. M., & Delcour, J. A. (2013). Relative importance of moisture migration and amylopectin retrogradation for pound cake crumb firming. *Food Chemistry*, *141*(4), 3960–3966. https://doi.org/10.1016/j.foodchem.2013.06.110

Marra, F., Zell, M., Lyng, J. G., Morgan, D. J., & Cronin, D. A. (2009). Analysis of heat transfer during ohmic processing of a solid food. *Journal of Food Engineering*, *91*(1), 56–63. https://doi.org/10.1016/j.jfoodeng.2008.08.015

Masure, H. G., Wouters, A. G. B., Fierens, E., & Delcour, J. A. (2019). Electrical resistance oven baking as a tool to study crumb structure formation in gluten-free bread. *Food Research International*, *116*, 925–931. https://doi.org/10.1016/j.foodres.2018.09.029

Olivera, D. F., Salvadori, V. O., & Marra, F. (2013). Ohmic treatment of fresh foods: Effect on textural properties. *International Food Research Journal*, *20*(4), 1617–1621.

Quarini, G. L. (1995). Thermalhydraulic aspects of the ohmic heating process. Journal of Food Engineering, 24(4), 561–574. https://doi.org/10.1016/0260-8774(95)90770-C

Salengke, S., & Sastry, S. K. (2007). Models for ohmic heating of solid-liquid mixtures under worst-case heating scenarios. *Journal of Food Engineering*, *83*(3), 337–355. https://doi.org/10.1016/j.jfoodeng.2007.03.026

Sarkis, J. R., Mercali, G. D., Tessaro, I. C., & Marczak, L. D. F. (2013). Evaluation of key parameters during construction and operation of an ohmic heating apparatus. Innovative Food Science and Emerging Technologies, 18, 145–154. https://doi.org/10.1016/j.ifset.2013.02.001

Sastry, Sudhir. K. (1992). A model for heating of liquid-particle mixtures in a continuous flow ohmic heater. *Journal of Food Process Engineering*, *15*(4), 263–278. https://doi.org/10.1111/j.1745-4530.1992.tb00156.x

Sastry, S K, & Palaniappan, S. (1992). Mathematical modelling and experimental studies on ohmic heating of liquid-particle mixtures in a static heater. *Journal of Food Process Engineering*, *15*(4), 241–261. https://doi.org/10.1111/j.1745-4530.1992.tb00155.x

Severini, C., & Derossi, A. (2016). Could the 3D Printing Technology be a Useful Strategy to Obtain Customized Nutrition? *Journal of Clinical Gastroenterology*, *50*(December), S175–S178. https://doi.org/10.1097/MCG.0000000000000705

Shim, J. Y., Lee, S. H., & Jun, S. (2010). Modeling of ohmic heating patterns of multiphase food products using computational fluid dynamics codes. *Journal of Food Engineering*, *99*(2), 136–141. https://doi.org/10.1016/j.jfoodeng.2010.02.009

Shynkaryk, M., & Sastry, S. K. (2012). Simulation and optimization of the ohmic processing of highly viscous food product in chambers with sidewise parallel electrodes. *Journal of Food Engineering*, *110*(3), 448–456. https://doi.org/10.1016/j.jfoodeng.2011.12.022

Srivastav, S., & Roy, S. (2014). Changes in electrical conductivity of liquid foods during ohmic heating. *International Journal of Agricultural and Biological Engineering*, *7*(5), 133–138. https://doi.org/10.3965/j.ijabe.20140705.015

Sun, J., Peng, Z., Zhou, W., Fuh, J. Y. H., Hong, G. S., & Chiu, A. (2015). A Review on 3D Printing for Customized Food Fabrication. *Procedia Manufacturing*, *1*, 308–319. https://doi.org/10.1016/j.promfg.2015.09.057

Sweat, V. E., & Parmelee, C. E. (1978). Measurement of thermal conductivity of dairy products and margarines. *Journal of Food Engineering*, *41*(2), 187–197. https://doi.org/10.1016/S0260-8774(99)00079-5

Tijskens, L. M. M., Hertog, M. L. A. T. M., & Nicolai, B. M. (2001). *Food Process Modelling*. *Woodhead Publishing Limited and CRC Press LLC, Cambridge, UK and Boca Raton, FL, USA*.

Yang, J., Wu, L. W., & Liu, J. (2001). *Rapid prototyping and fabrication method for 3-D food objects, Nanotek Instruments, Inc., Opelika, AL (US), US Patent 6,280,785 B1*.

Yildiz, H., & Guven, E. (2014). Industrial applications and potential use of ohmic heating for fluid foods. *Bulgarian Chemical Communications*, *46*, 98–102. http://bcc.bas.bg/BCC_Volumes/Volume_46_Special_B_2014/BCC-46-B-98-102.pdf

Zhang, L., & Fryer, P. J. (1993). Models for the electrical heating of solid-liquid food mixtures. *Chemical Engineering Science*, *48*(4), 633–642. https://doi.org/10.1016/0009-2509(93)80132-A

Zhou, J. (2004). Microwave Assisted Moulding of Starch-Based Foams. In *PhD Thesis, Brunel University, London, England UK* (p. 223).

696

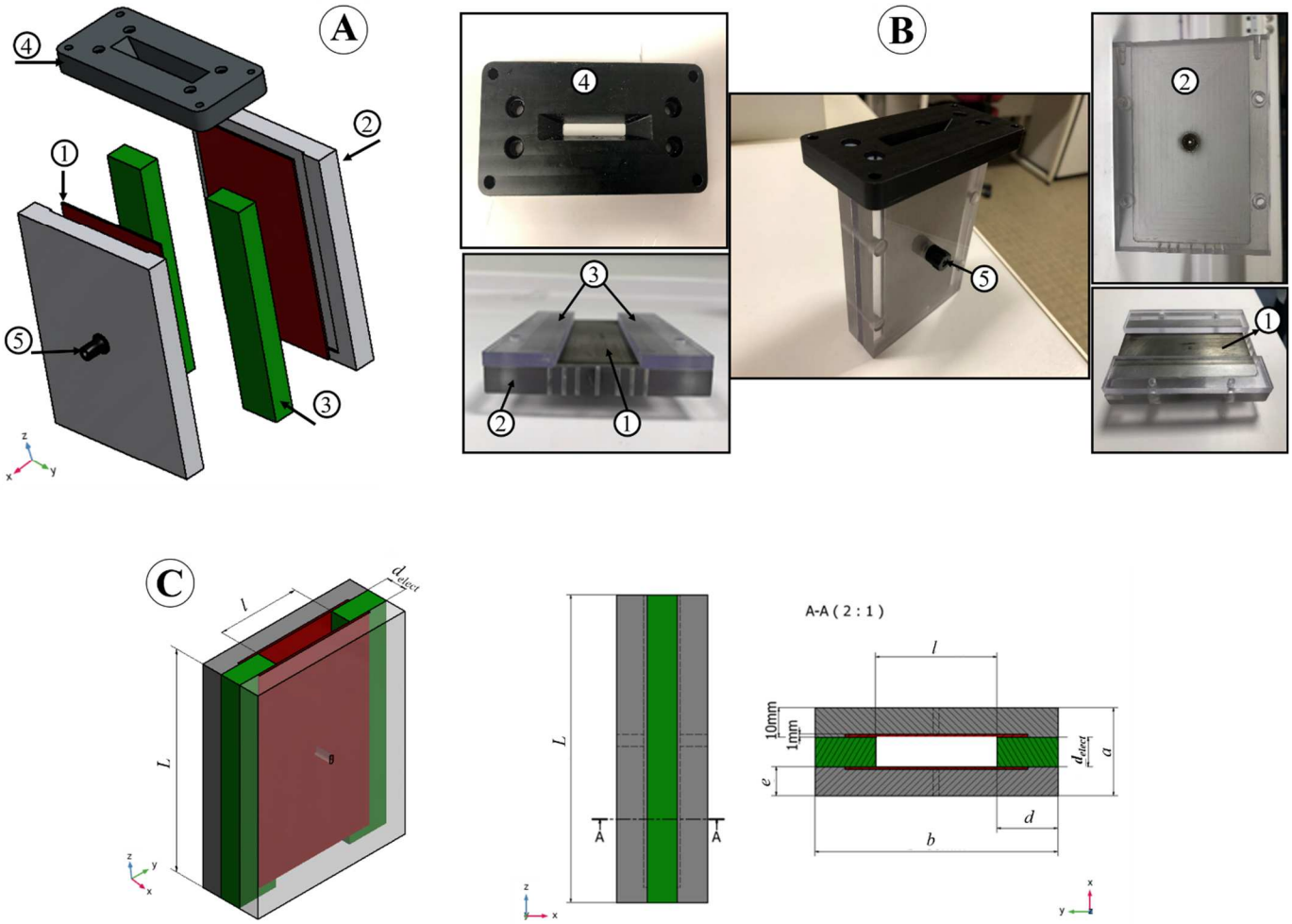

697 **Fig. 1.** (A) Schematic of 3D nozzle geometry, consisted of ; (1) electrodes (red), (2) plates (grey), (3) beam
698 (green), (4) channel support (black), (5) electric relays. (B) Different parts of the reel nozzle, same numbers as in
699 (A). (C) Section views of the rectangular channel, distance between electrodes (d_{elect}) along the x-axis, nozzle
700 width (l) along the y-axis; nozzle length (L) along the z-axis.

701

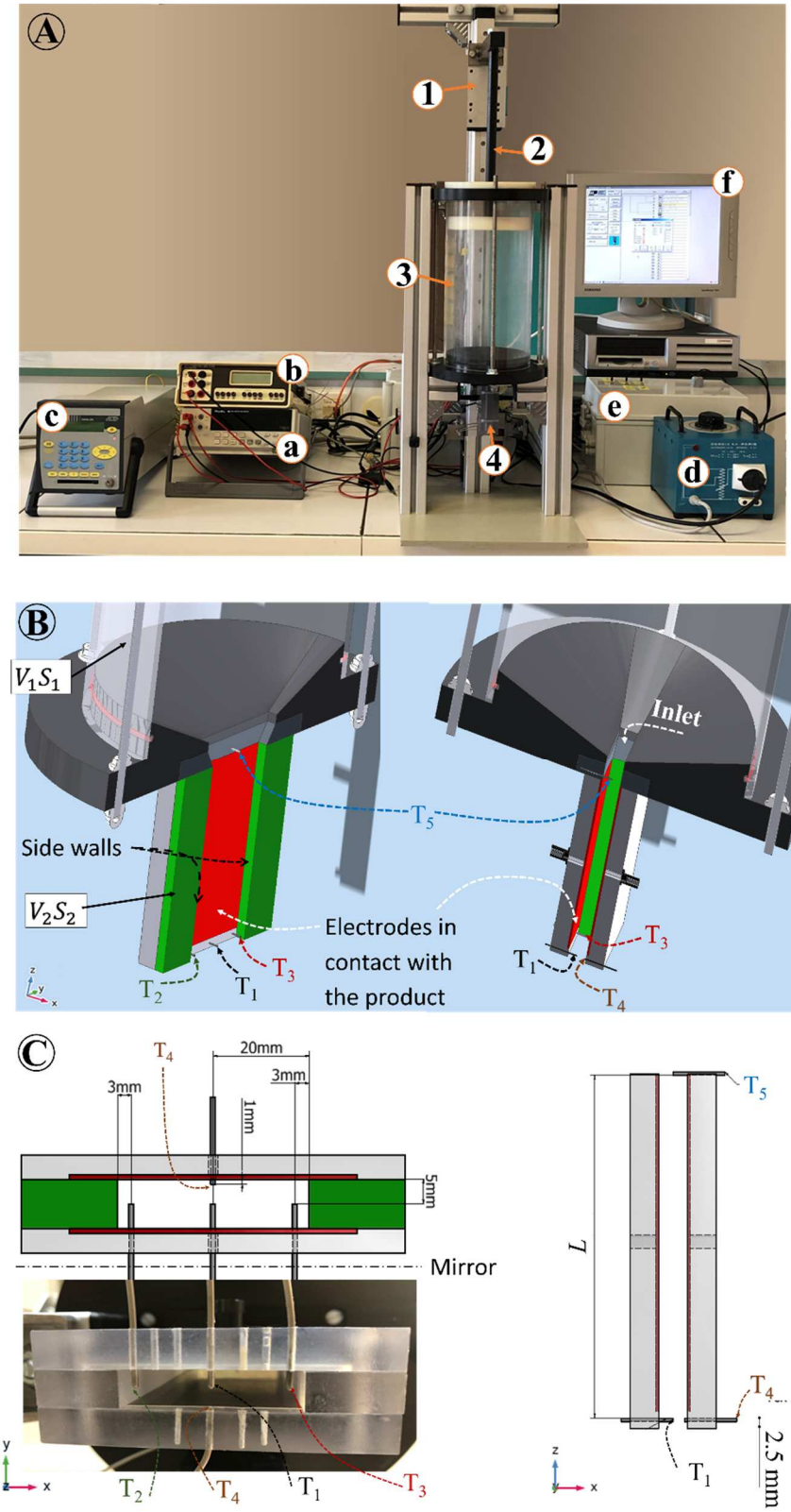

Fig. 2. (A) Overall installation of the system used for experiments, composed of mechanical parts: (1) drive motor, (2) piston, (3) cylindrical container, and (4) nozzle with ohmic heating, and electrical parts: (a) voltmeter, (b) ammeter, (c) data logger, (d) autotransformer, (e) motor controller, and (f) PC. (B) 3D views of the location of the thermocouples in the product along the nozzle; V_1 and S_1 are the velocity of the batter and surface of the cylindrical container (3), V_2 and S_2 are the velocity of the batter and surface of the nozzle (4). (C) Location of each thermocouple at the nozzle outlet and inlet.

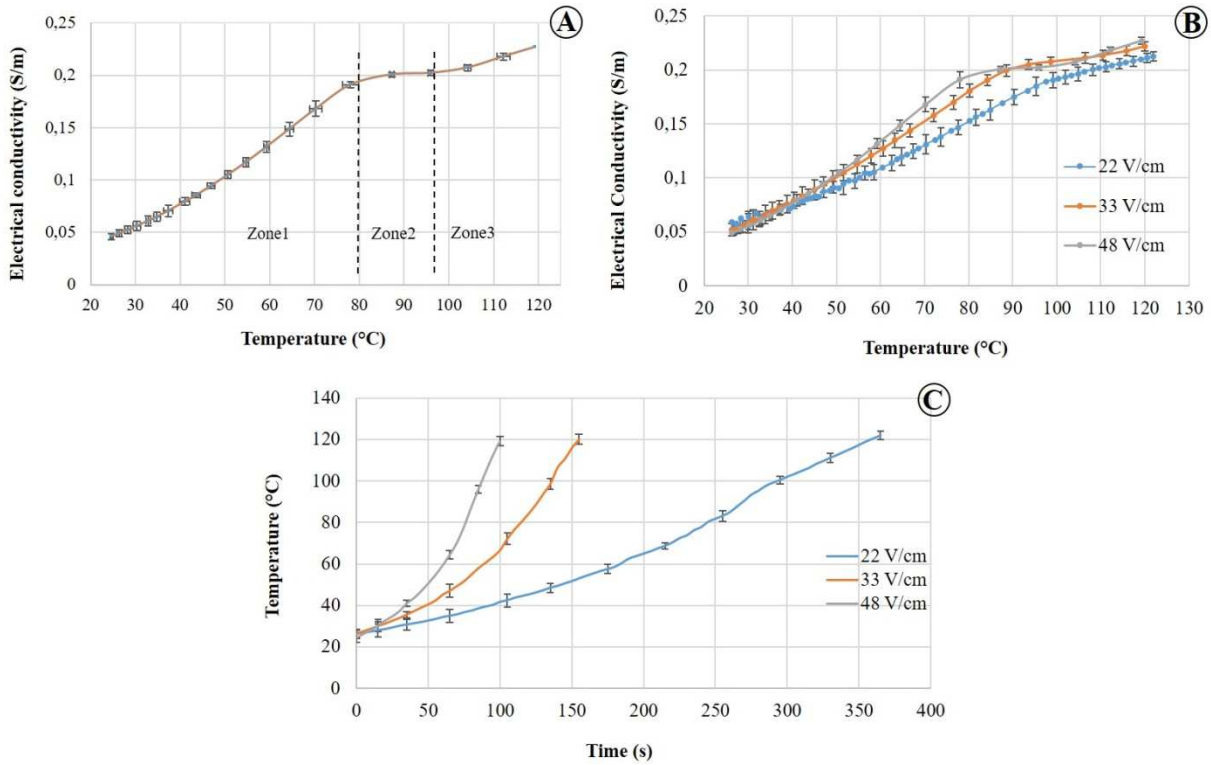

Fig. 3. (A) Electrical conductivity of the batter vs. temperature at a voltage gradient of 50 V/cm, (B) electrical conductivity of the batter vs. temperature at three different voltage gradients (22 V/cm (100 V), 33 V/cm (150 V), and 48 V/cm (200 V)) and (C) evolution of core temperature vs. time for the three different voltages.

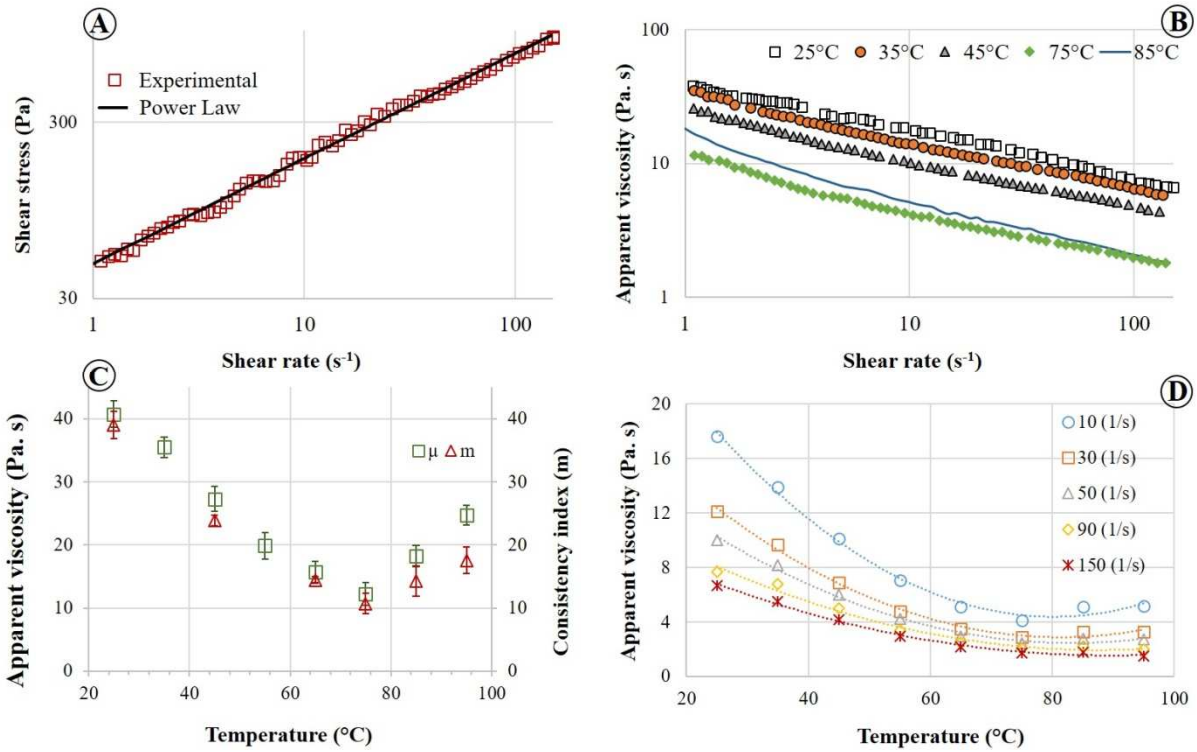

Fig. 4. (A) Evolution of the batter shear stress vs. shear rate at 25 °C, in logarithmic form, (B) cake batter apparent viscosity vs. shear rate at five different temperatures, in logarithmic form, (C) consistency index and apparent viscosity at 1 s^{-1} vs. temperature, and (D) apparent viscosity vs. temperature at five different shear rates.

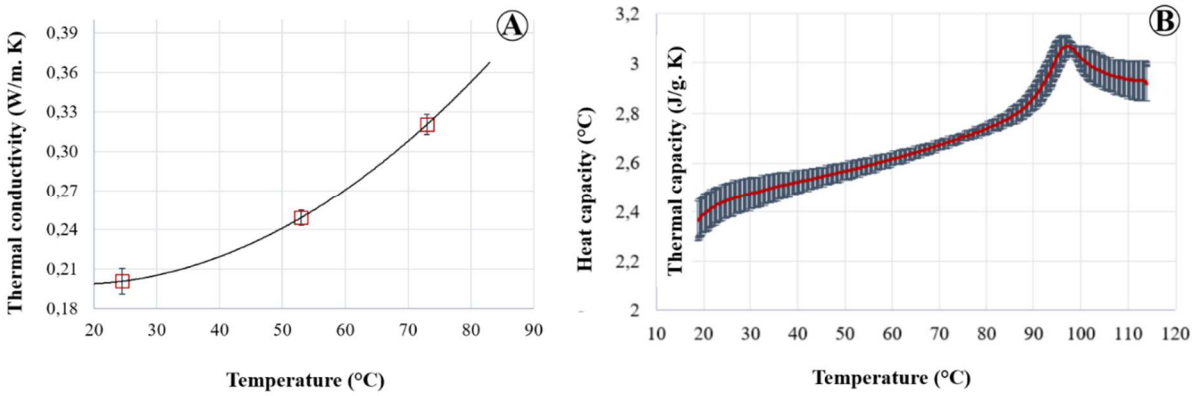

729
730 **Fig. 5** (A) Thermal conductivity and (B) heat capacity of the cake batter vs. temperature.
731
732

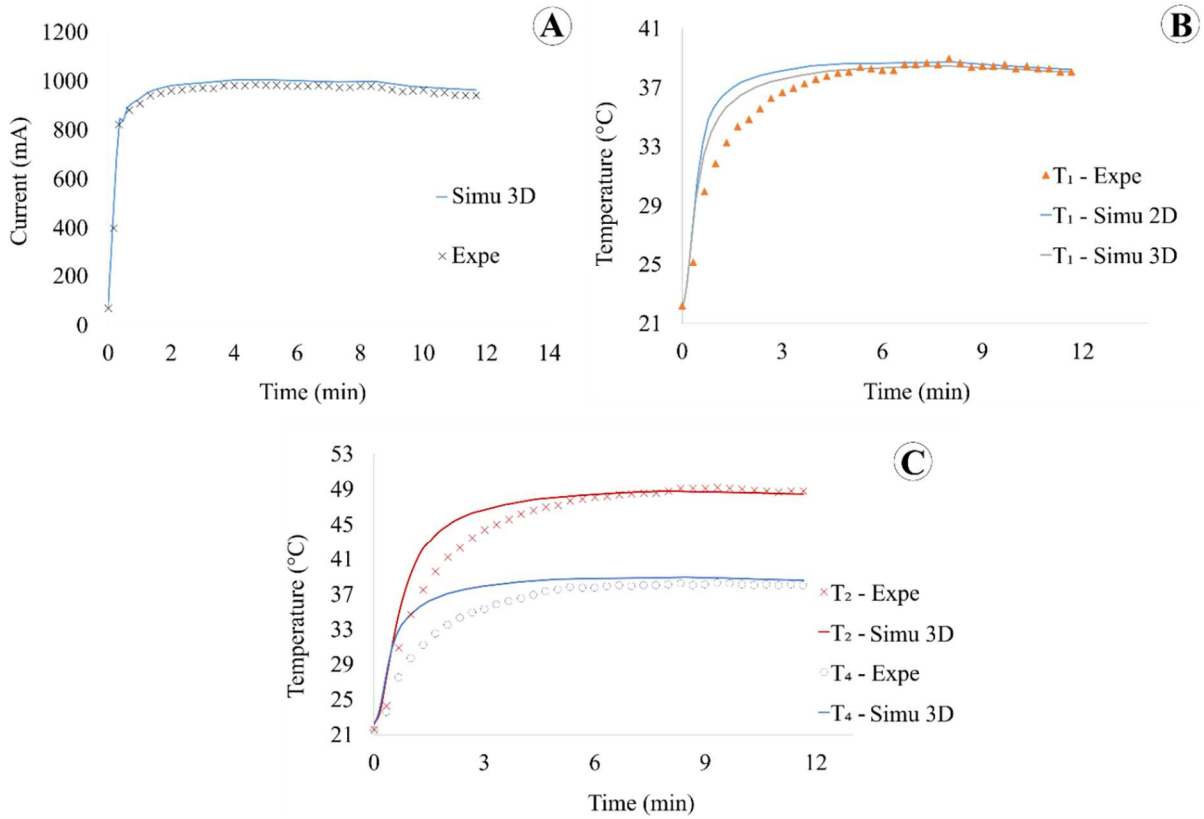

Fig. 6 Validation of the model: experimental and modelled data for (A) the current evolution between electrodes, (B) temperature measurements at the outlet (T_1), and (C) temperatures T_2 and T_4 vs. time at the nozzle outlet for 12 min of injection at 65 V.

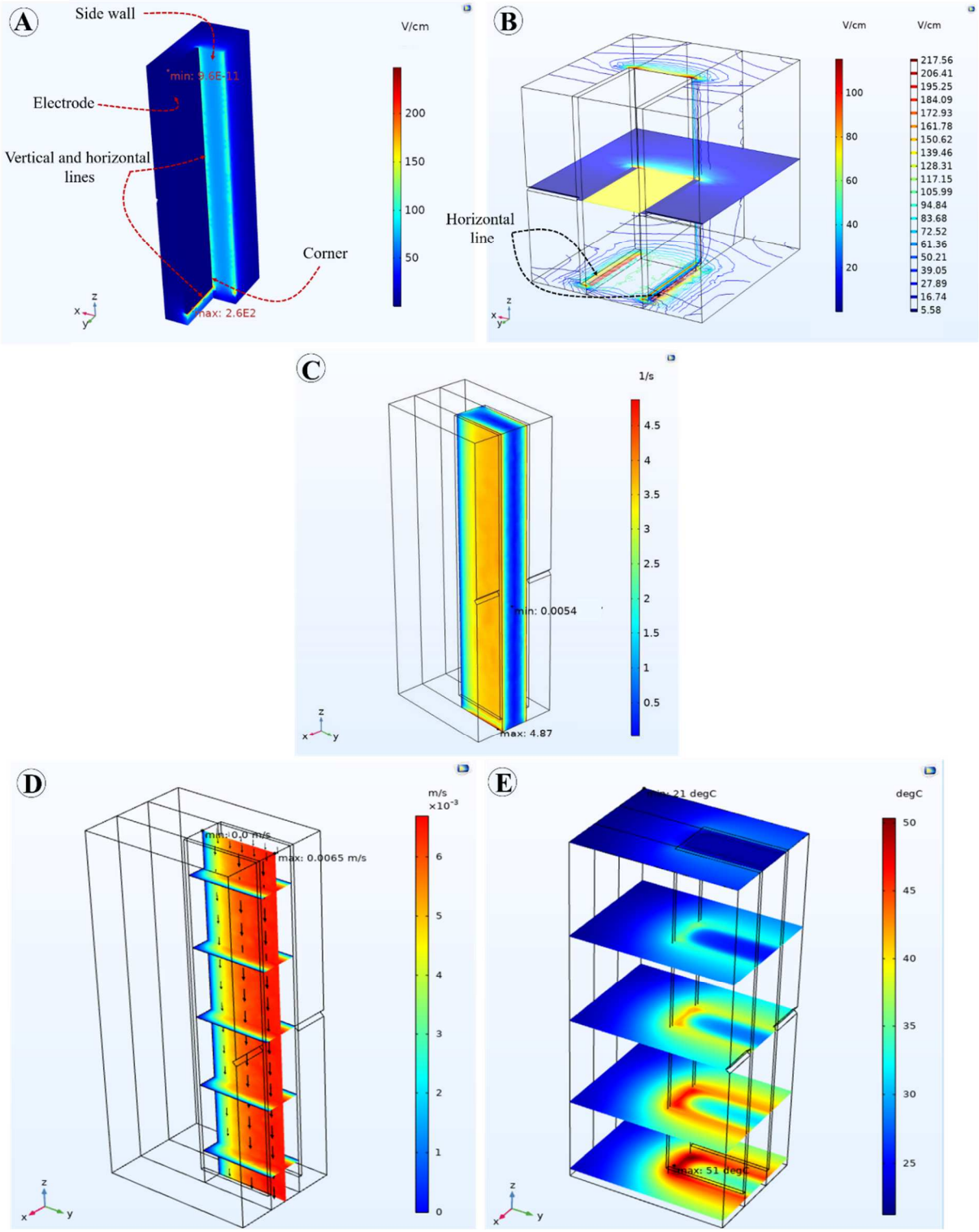

Fig. 7. Plots for the cake batter after 12 min heating at 65 V and 4 mm/s, for (A) volume electric field; (B) electric field in the xy plane; (C) volume shear rate; (D) velocity along the y axis; and (E) temperature distribution in the nozzle in the xy plane at different location along z axis.

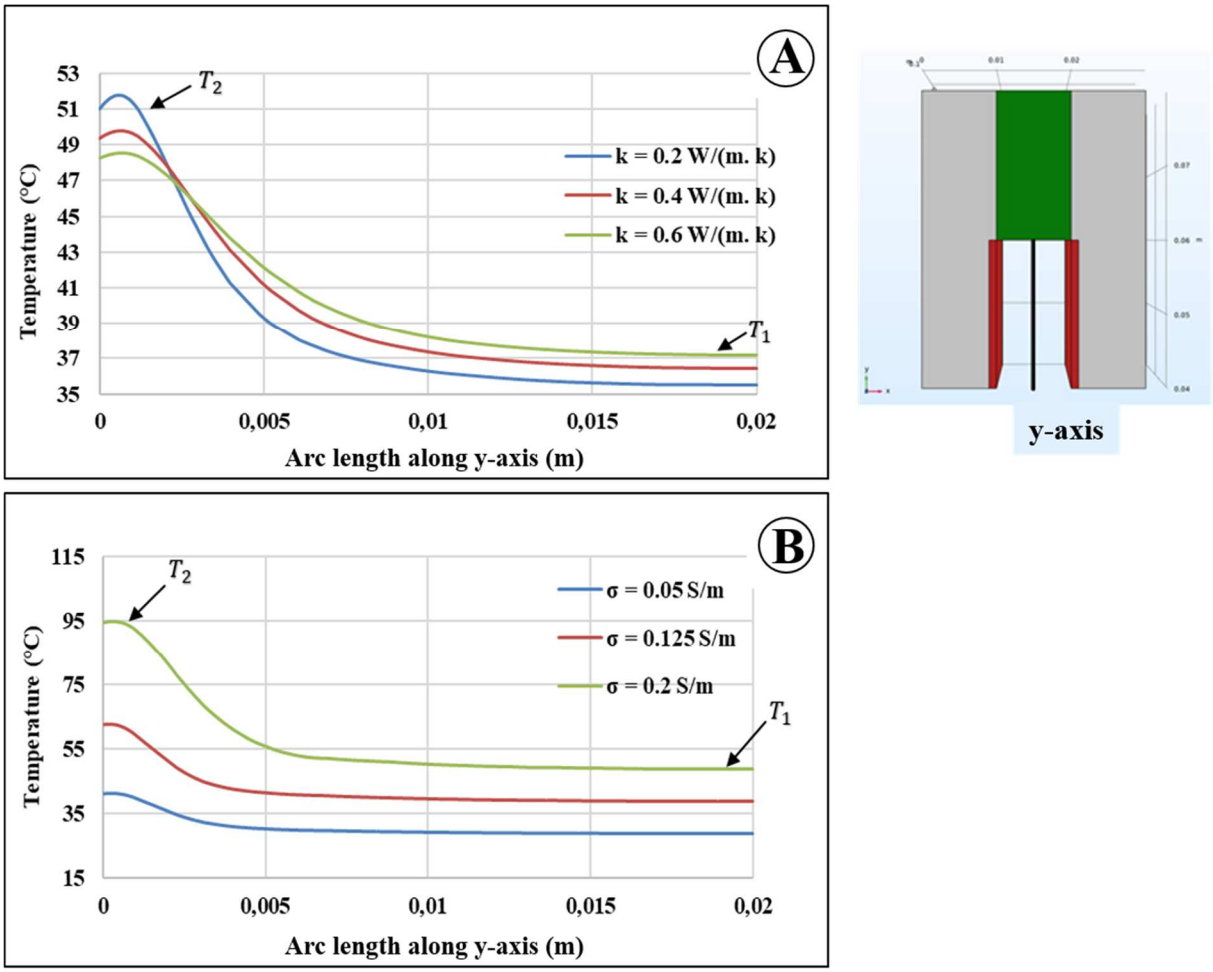

Fig. 8. Parametric study of (A) thermal conductivity for 65 V – 4 mm/s, (B) electrical conductivity for 65 V- 12 mm/s, and their effects on the outlet temperature profile along the y-axis.

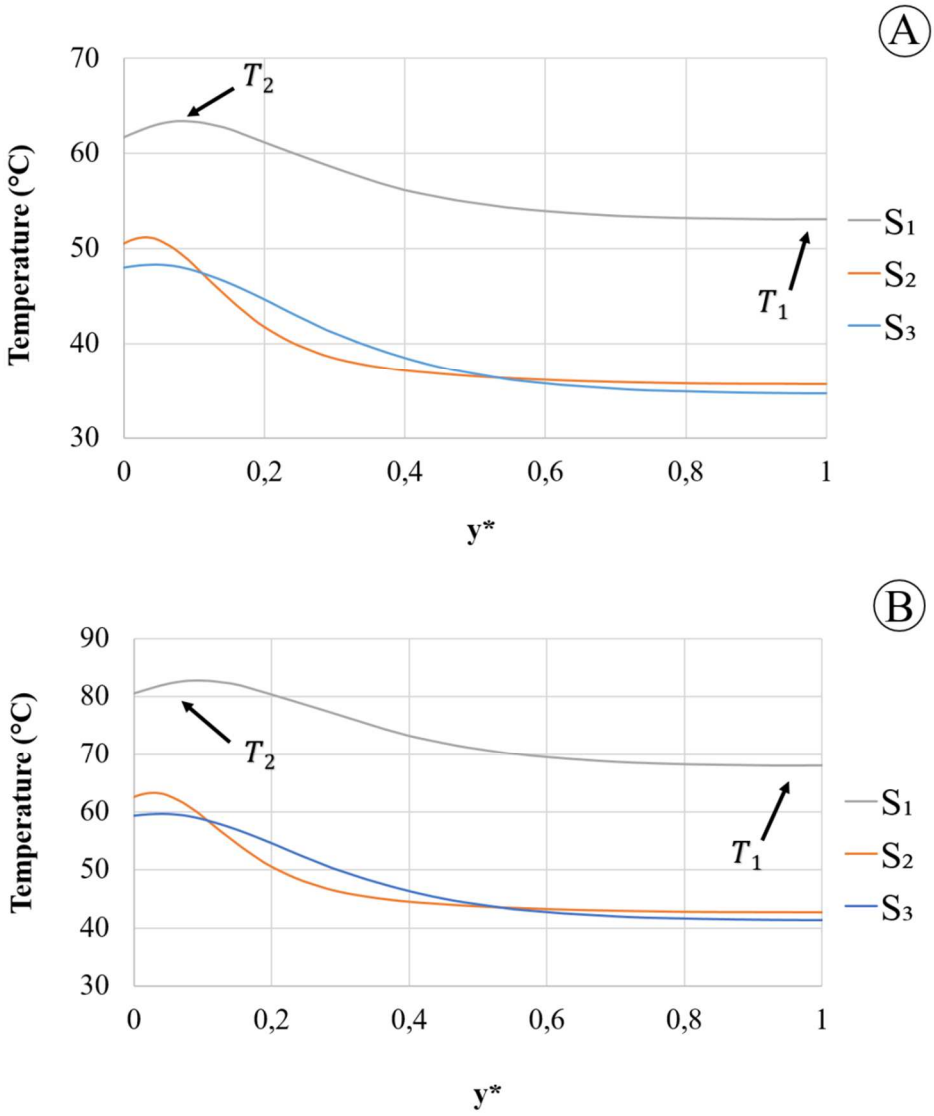

Fig. 9. Temperature profiles vs non-dimensional coordinate $y^* = y/(l/2)$ for three different nozzle sections: S_1= 1 cm^2, S_2 = 4 cm^2 and S_3 = 2 cm^2) with aspect ratios ($\alpha = d_{elect}/l$) equal to 0.25, 0.25 and 0.5 respectively, and for two voltages: (A) 65 V/cm, and (B) 100 V/cm, at a velocity of 4 mm/s.